PLK1 phosphorylates PAX3-FOXO1 the inhibition of which triggers regression of alveolar rhabdomyosarcoma

Thalhammer, Verena ; Lopez-Garcia, Laura A ; Herrero Martín, David ; Hecker, Regina ; Laubscher, Dominik ; Gierisch, Maria E ; Wachtel, Marco ; Bode, Peter ; Nanni, Paolo ; Blank, Bernd ; Koscielniak, Ewa ; Schäfer, Beat W

Abstract: Pediatric tumors harbor very low numbers of somatic mutations and therefore offer few targets to improve therapeutic management with targeted drugs. In particular, outcomes remain dismal for patients with metastatic alveolar rhabdomyosarcoma (aRMS), where the chimeric transcription factor PAX3/7-FOXO1 has been implicated but problematic to target. In this report, we addressed this challenge by developing a two-armed screen for druggable upstream regulatory kinases in the PAX3/7-FOXO1 pathway. Screening libraries of kinome siRNA and small molecules, we defined PLK1 as an upstream-acting regulator. Mechanistically, PLK1 interacted with and phosphorylated PAX3-FOXO1 at the novel site S503 leading to protein stabilization. Notably, PLK1 inhibition led to elevated ubiquitination and rapid proteasomal degradation of the PAX3-FOXO1 chimeric oncoprotein. On this basis, we embarked on a preclinical validation of PLK1 as target in a xenograft mouse model of aRMS, where the PLK1 inhibitor BI 2536 reduced PAX3-FOXO1-mediated gene expression and elicited tumor regression. Clinically, analysis of human aRMS tumor biopsies documented high PLK1 expression to offer prognostic significance for both event-free and overall survival. Taken together, these preclinical studies validate the PLK1 - PAX3-FOXO1 axis as a rational target to treat alveolar rhabdomyosarcoma.

DOI: https://doi.org/10.1158/0008-5472.CAN-14-1246

PLK1 phosphorylates PAX3-FOXO1 the inhibition of which triggers regression of alveolar rhabdomyosarcoma

Verena Thalhammer[1], Laura A. Lopez-Garcia[1], David Herrero-Martin[1], Regina Hecker[1], Dominik Laubscher[1], Maria E. Gierisch[1], Marco Wachtel[1], Peter Bode[2], Paolo Nanni[3], Bernd Blank[4], Ewa Koscielniak[4], and Beat W. Schäfer[1]

[1]Department of Oncology and Children's Research Center, University Children's Hospital Zurich, Zurich, Switzerland
[2]Department of Surgical Pathology, University Hospital Zurich, Zurich, Switzerland
[3]Functional Genomics Center Zurich, University of Zurich, Zurich, Switzerland
[4]Department of Oncology/Hematology/Immunology, Olgahospital, Klinikum Stuttgart, Stuttgart, Germany

Running title: Targeting of PAX3-FOXO1 by PLK1 inhibition

Keywords: PLK1, PAX3-FOXO1, posttranslational modifications, aRMS, prognostic marker

Financial support: Swiss National Science Fund (31003A-138460)
Swiss Research Foundation Child and Cancer
Cancer League of the Kanton Zurich
Forschungskredit University of Zurich

Corresponding author: Beat W. Schäfer
Department of Oncology, Children's Hospital Zurich
Steinwiesstrasse 75
8032 Zurich, Switzerland
Beat.Schaefer@kispi.uzh.ch
Phone: +41 (44) 266 7553 Fax: +41 (44) 634 8859

No Disclosures

Word count: 4946

Figures and Tables: 6 Figures (colored), 1 Table
7 Supplementary Figures (colored), 3 Supplementary Tables

Abstract

Pediatric tumors harbor very low numbers of somatic mutations and therefore offer few targets to improve therapeutic management with targeted drugs. In particular, outcomes remain dismal for patients with metastatic alveolar rhabdomyosarcoma (aRMS), where the chimeric transcription factor PAX3/7-FOXO1 has been implicated but problematic to target. In this report, we addressed this challenge by developing a two-armed screen for druggable upstream regulatory kinases in the PAX3/7-FOXO1 pathway. Screening libraries of kinome siRNA and small molecules, we defined PLK1 as an upstream-acting regulator. Mechanistically, PLK1 interacted with and phosphorylated PAX3-FOXO1 at the novel site S503 leading to protein stabilization. Notably, PLK1 inhibition led to elevated ubiquitination and rapid proteasomal degradation of the PAX3-FOXO1 chimeric oncoprotein. On this basis, we embarked on a preclinical validation of PLK1 as target in a xenograft mouse model of aRMS, where the PLK1 inhibitor BI 2536 reduced PAX3-FOXO1-mediated gene expression and elicited tumor regression. Clinically, analysis of human aRMS tumor biopsies documented high PLK1 expression to offer prognostic significance for both event-free and overall survival. Taken together, these preclinical studies validate the PLK1 - PAX3-FOXO1 axis as a rational target to treat alveolar rhabdomyosarcoma.

Introduction

Rhabdomyosarcoma is the most common pediatric soft tissue sarcoma and can be divided into two main subgroups with different outcomes reflecting distinct genetic backgrounds. Alveolar rhabdomyosarcoma (aRMS) is more aggressive than embryonal rhabdomyosarcoma (eRMS) and often displays resistance to conventional chemo- and radiotherapy resulting in a 5-year survival rate of only 30% (1). Until now, there are no alternative therapeutic strategies to these conventional treatments. Searching for appropriate molecular targets, large proteomic screening and sequencing approaches have been undertaken showing that pediatric tumors harbor far fewer somatic mutations than adult tumors (2). In contrast to eRMS, analyzing genetic landscapes of alveolar rhabdomyosarcoma even further minimized the number of potential targets and excluded enrichment of any mutated oncogenic canonical pathway in the majority of patients (3, 4). These findings indicate that aRMS is driven by very few individual oncogenes and consequently reinforce the focus on the role of the tumor specific chimeric transcription factor PAX3/7-FOXO1.

The fusion protein is expressed in about 80% of aRMS tumors suggesting a dominant role as oncogenic driver (4, 5). Its transforming capacity (6, 7) is underlined by the ability to affect multiple oncogenic downstream pathways (8-13). Furthermore, aRMS is addicted to expression of the fusion protein as its continuous activity is essential for maintaining tumor cell survival (14, 15). Finally, its presence has also important prognostic significance (16, 17). PAX3-FOXO1 is, in conclusion, a highly relevant potential target and offers the opportunity for development of novel directed therapies. However, directly antagonizing transcription factors remains a pharmaceutical challenge and alternative indirect strategies interfering with the regulatory network of the fusion protein need to be developed.

PAX3-FOXO1 is characterized by high expression, exclusive nuclear subcellular localization, enhanced protein stability, and increased transcriptional activity compared

to wild type PAX3 or FOXO1 (18-22). Currently, we aim to mechanistically understand these different levels of regulation required for the oncogenic function. We, as well as others, were able to demonstrate that the transcriptional activity of PAX3-FOXO1 depends on its phosphorylation state providing novel therapeutic opportunities (23-25).

Polo-like kinase 1 (PLK1) is known as key regulator of mitosis with critical roles in mitotic entry, centrosome maturation, cohesin release, bipolar spindle formation, mitotic exit, and cytokinesis. Overexpression of PLK1 is linked to poor prognosis in a variety of different cancers (26, 27). In contrast to healthy cells, it localizes to the nucleus already before G2-M in cancer cells and can be detected during the entire interphase (28). Therefore, cancer-cell specific functions in G1-S transition and DNA replication are suggested beyond its role in regulation of mitosis. Interestingly, PLK1 is associated with PI3K and MAPK pathways, both of which are thought to play important roles in aRMS (29, 30). Hence, PLK1 overexpression might not just be a consequence of enhanced proliferation, but it is likely that PLK1 actively contributes to early carcinogenesis. However, a specific role for PLK1 in aRMS has not yet been described.

Here, we utilized a two-armed screening strategy to identify PLK1 as upstream regulator of PAX3-FOXO1, whereby PLK1 phosphorylated and subsequently stabilized the fusion protein. Since we observed objective regression of xenograft tumors upon PLK1 inhibition and found that PLK1 expression in patient biopsies has significant prognostic value, we propose the PLK1 – PAX3-FOXO1 axis to be a very promising novel target for aRMS therapy.

Material and Methods

Cell lines

The aRMS cell lines Rh4, Rh41 (Peter Houghton, St. Jude Children's Hospital, Memphis, TN, USA), RMS13 (Roland Kappler, Ludwig–Maximilian University Munich, Germany), Rh3, Rh5, Rh10 (Susan Ragsdale, St. Jude Children's Hospital, Memphis, TN, USA), CW9019 (Soledad Gallego, Hospital Universitari Vall d'Hebron, Barcelona, Spain) and Rh30 as well as HEK293T cells (American Type Culture Collection ATCC, LGC Promochem, Molsheim Cedex, France) were cultured in Dulbecco's modified Eagle's medium (Sigma-Aldrich, Buchs, Switzerland), supplemented with 100 U/ml penicillin/streptomycin, 2 mM L-glutamine and 10% FBS (Life Technologies, Zug, Switzerland) in 5% CO_2 at 37°C. RD and Rh36 eRMS cells were kindly provided by Peter Houghton (St. Jude Children's Hospital, Memphis, TN, USA). Ruch2 and Ruch3 cell lines were established in our laboratory (31).

aRMS and eRMS cell lines were tested and authenticated by cell line typing analysis (STR profiling) in 2011/2014 and positively matched (32).

Plasmids and transfection methods

Plasmids and transfection methods are described in Supplementary Material and Methods.

siRNA kinome library screens and data analysis

A kinome siRNA library targeting 719 kinases was used (Ambion Silencer® V3 Kinase siRNA Library, Life Technologies, Zug, Switzerland) together with a sub-library targeting 47 kinases (Ambion Silencer® Select Costum siRNA Library, Life Technologies) with 3 unique siRNA sequences per gene. Ambion non-targeting siRNA served as negative control, whereas PAX3-FOXO1 break-point specific siRNA (33), luciferase specific siRNA (pGL4, Custom Select) and KIF11 siRNA (AM4639; all Ambion, Life Technologies) were

used as positive controls. Reverse transfection was carried out with $1x10^4$ cells per 96-well at a final concentration of 50 nM using N-TER nanoparticle transfection reagent (Sigma-Aldrich). Luciferase activity was determined by the Luciferase Assay System E1501 (Promega, Dübendorf, Switzerland) 48h post transfection and values normalized to viable cell numbers determined by WST-1 assay (Roche Diagnostics, Rotkreuz, Switzerland). Measurements were normalized using the per-plate median normalization method (excluding controls). Triplicate median-normalized luciferase values were averaged for each kinase before calculating the ratio to the averaged WST-1 absorbance (normalized luciferase activity). Cell viability of Rh4 and RMS13 cells was measured 72h post transfection using WST-1. Both screens were done in triplicates and non-targeting, PAX3-FOXO1, pGL4 and KIF11 siRNAs were included in duplicates on each plate.

Small-molecule compounds screen and dose response studies

A small-molecule compound library (Supplementary Tab. S2) covering 161 different inhibitors was used to treat $5x10^3$ Rh4-AP2-LF cells per 96-well 24h after plating at a final concentration of 500 nM for 24h. Luciferase activity/cell viability ratio was determined as described above. For dose response curves, this ratio was plotted against the logarithm of drug concentrations and IC_{50} values were calculated by nonlinear regression curve fitting using GraphPad Prism software (GraphPad Software Inc., San Diego, CA, USA).

PLK1 silencing and small-molecule inhibition

Knockdowns of PLK1 and PLK4 were achieved by reverse transfection of $1.9\text{-}3.8x10^5$ cells in 6-well plates using scrambled (4390846) or PLK1 and PLK4 directed siRNAs (25 nM 1341, 8 nM S449, 25 nM S21083; all Ambion, Life Technologies) with INTERFERin™ according to the manufacturer's protocol (Polyplus-Transfections, Illkirch, France). Cells were lysed 48h post transfection.

$2x10^5$ cells per 6-well were treated 24h after seeding with 15 nM BI 2536 (Axon Medchem, Groningen, Netherlands) or 20 nM BI 6727 (Selleck Chemicals, Houston TX, USA). Cells were lysed for RNA or protein extraction after 48h. For proteasomal degradation studies, 10 nM - 50 nM Bortezomib (Cilag, Schaffhausen, Switzerland) was simultaneously added and cells were lysed after 20h.

qRT- PCR

Total RNA was extracted using the Qiagen RNeasy Kit (Qiagen, Basel, Switzerland) and reverse-transcribed using oligo (dT) primers and Omniscript reverse transcriptase (Qiagen). qRT-PCR was performed for PLK1 (Hs00153444_m1), PLK4 (Hs00179514_m1), PAX3-FOXO1 (Hs03024825_ft), AP2β (Hs00231468_m1), FGFR4 (Hs01106908_m1), CDH3 (Hs00999918_m1), PIPOX (Hs04188864_m1) and MYL1 (Hs00984899_m1) using TaqMan gene expression master mix (all Life Technologies). Cycle threshold (C_T) values were normalized to GAPDH (Hs02758991_g1). Relative expression levels were calculated using the $\Delta\Delta C_T$ method based on experiments performed in triplicates. Geometric mean values and the 95% confidence interval were calculated based on four to six biological replicates.

Immunoblotting

Total cell extracts were separated using 4-12% Bis-Tris SDS-PAGE gels (Life Technologies) and transferred to nitrocellulose membranes (PROTAN, Schleicher & Schuell, Kassel, Germany). After blocking with 5% milk powder in TBS/0.1% Tween, membranes were incubated with primary antibodies overnight at 4°C. After washing in TBS/0.1% Tween, membranes were incubated with IgG HRP-linked antibody for one hour at room temperature. Proteins were detected using ECL detection reagent (Fisher Scientific, Wohlen, Switzerland) after washing in TBS/0.1% Tween.

Antibodies

Antibodies are described in Supplementary Material and Methods.

Co-immunoprecipitation

Cells from one confluent 10 cm dish were lysed in 1 ml lysis buffer and incubated for 10 min at 4°C with Dynabeads® Protein G (Novex by Life Technologies) coupled to indicated antibodies. Beads were washed three times with lysis buffer, proteins eluted in 1x NuPAGE LDS sample buffer (Life Technologies) at 70°C and analyzed by Western blotting.

Stability assay

$2x10^5$ RD cells were seeded per 6-well the day before transfection with 1 µg pMSCV-PAX3-FOXO1-IRES-GFP or pMSCV-PAX3-FOXO1-S503A-IRES-GFP. Cells were treated with 35 µM cycloheximide (Sigma-Aldrich) or DMSO for 6h before lysis and protein extraction. Protein levels were analyzed by Western blotting.

Purification of FLAG-PAX3-FOXO1

Rh4, RMS13 or HEK293T cells were transfected with pCMV-NFLAG-PAX3-FOXO1 in 15 cm plates, lysed 40h post transfection and FLAG-PAX3-FOXO1 was immunoprecipitated using 75 µl Dynabeads® per plate coupled to 8 µg monoclonal ANTI-FLAG® M2 antibody. After washing, bead-bound FLAG-PAX3-FOXO1 was either used for *in vitro* kinase assays or the protein was eluted by 1x NuPage LDS buffer and directly subjected to mass spectrometry.

***In vitro* kinase assay and mass spectrometry**

Bead-bound protein was dephosphorylated using 300 units CIAP enzyme (alkaline phosphatase, calf intestinal HC, Promega, Dübendorf, Switzerland) for 90 min at 37°C

(50 mM Tris HCl pH 7.5, 1 mM $MgCl_2$, 0.1 mM $ZnCl_2$). FLAG-PAX3-FOXO1 was phosphorylated after washing using 500 ng or 2.5 µg of recombinant PLK1 (Life Technologies) for 30 min at 30°C (250 mM HEPES pH 7.5, 50 mM $MgCl_2$, 12.5 mM DTT, 0.05% Triton X-100, 200 µM ATP). 4x NuPage LDS buffer was added for elution and proteins were separated by gel electrophoresis. After staining with colloidal coomassie (Instant blue, Expedeon, Harston, UK), the band corresponding to FLAG-PAX3-FOXO1 was excised and prepared for mass spectrometry as described in Supplementary Material and Methods.

Ubiquitination studies

Rh4 cells were transfected with pCMV-FLAG-PAX3-FOXO1 plasmid and pCDNA3-HA-Ubiquitin at a ratio of 1:2 for 48h. Cells were treated with 200 nM PLK1 inhibitors for 21h prior to addition of 10 µM MG-132 (Calbiochem, Millipore, Zug, Switzerland) for 5h. After lysis (2% SDS, 150 mM NaCl, 10 mM Tris/HCl, 2 mM Na_3VO_4, 50 mM NaF), samples were boiled for 10 min, sonicated, diluted with 9 volumes of dilution buffer (150 mM NaCl, 10 mM Tris/HCl, 2 mM EDTA, 1% TritonX) and incubated for 30 min at 4°C. IP was performed using Dynabeads® coupled to ANTI-FLAG® M2 antibody for 1h at 4°C. Beads were washed three times with lysis buffer, proteins eluted with 3x FLAG peptide (Sigma-Aldrich) and analyzed by Western blotting.

Xenograft studies

$5x10^6$ Rh4, Rh4luc or RMS13luc cells were engrafted subcutaneously in 6 weeks old NOD/Scid il2rg$^{-/-}$ mice (male and female, 20-25 g, Charles River, Sulzfeld, Germany). Mice bearing established tumors with volumes of 65 – 470 mm^3 were treated intravenously with either sterile 0.9% NaCl or BI 2536 at 40 mg/kg on two consecutive days weekly for three cycles. BI 2536 was formulated in hydrochloric acid (0.1 N) diluted with 0.9% NaCl (34). Total tumor volumes were determined either by measuring

two diameters (d1, d2) in right angles using a digital caliper ($V= (4/3) \pi r^3$; r= (d1+d2)/4) or by *in vivo* imaging. D-luciferin (Caliper Life Sciences, Oftringen, Switzerland) was injected intraperitoneally (10 µl/g body weight), and tumors were monitored by the IVIS Lumina XR imaging system (Caliper Life Sciences). Control mice were euthanized when reaching a tumor volume of 1000 mm^3.

Immunohistochemistry

Three-micron thick sections of formalin-fixed, paraffin-embedded tissue were mounted on glass slides (SuperFrost Plus; Menzel, Braunschweig, Germany), deparaffinized, rehydrated and stained with hematoxylin and eosin (H&E). Immunohistochemical stainings were performed using the Ventana Benchmark system (Ventana Medical Systems, Tucson, AZ) and Ventana UltraView DAB reagents.

Tissue arrays

Tissue arrays have been previously described (35, 36). Immunohistochemistry was performed on Leica BondMax instruments using Refine HRP-Kits (Leica DS9800, Leica Microsystems Newcastle, Ltd.). Paraffin-slides were dewaxed, followed by pretreatment (Epitop Retrieval Buffer 2, 45 min, 100°C) and incubated with anti-PLK1 antibody (1:600). Tumors showing at least 1-5% of cells with a very high staining intensity were assigned to the high expression group. In contrast, tumors with low expression showed homogenous overall staining of reduced intensity. TMAs were analyzed double-blinded.

Results

Kinome-wide siRNA screen identifies PAX3-FOXO1 regulators

To identify kinases regulating the activity of the oncogenic transcription factor PAX3-FOXO1, we established a stable reporter cell line to monitor fusion protein activity (Fig. 1A). Rh4 aRMS cells with a transcriptome very similar to tumor biopsies (13) were stably transfected with a PAX3-FOXO1-responsive luciferase reporter employing a well-characterized endogenous AP2β promoter fragment (10) to generate Rh4-AP2β-LF cells. Depletion of PAX3-FOXO1 by siRNA (33) or silencing of luciferase itself resulted in a more than 70% decrease in luciferase activity (Supplementary Fig. S1A). Therefore, this reporter assay constitutes a valid tool for functional screening of PAX3-FOXO1 upstream regulators.

First, we performed a kinome-wide siRNA screen (Figure 1A). Rh4-AP2β-LF cells were transfected with three unique siRNA sequences targeting each of the 719 kinases (Fig. 1B and Supplementary Fig. S1B). PAX3-FOXO1, KIF11 (mitotic motor protein) and luciferase control siRNAs were included on each plate and the ratio of luciferase activity to cell viability from averaged triplicate values was determined for each siRNA. Only siRNAs that reduced this ratio by at least 1.5 SDs from the mean of the luciferase control were considered as potential candidates. Applying this criterion for at least two independent siRNAs, we identified 47 candidates that potentially contribute to the activity of PAX3-FOXO1 (Supplementary Tab. S1). Importantly, these kinases are all expressed in Rh4 cells and primary aRMS tumors, at least at the mRNA level (9, 13).

To narrow down the list of candidates, we applied a secondary viability screen using an siRNA library containing three additional targeting sequences per kinase (sequence panels A, B and C). We determined mean relative cell viability after individual silencing for 72 hours in Rh4 and RMS13 cells. Next to two positive controls (PAX3-FOXO1 and KIF11) included on each screening plate, we found that knockdown of PLK1 clearly had the strongest impact on cell viability in both cell lines (up to 61% reduction), whereas

the per-plate means reached only 7% to 22% (Fig. 1C). These results suggest that PLK1 expression might be important for aRMS cell survival.

Small-molecule inhibitor screen reveals PLK1 as potential PAX3-FOXO1 regulator

In parallel to the siRNA screen, we conducted a small-molecule, mainly kinase-directed drug screen, to further examine the regulation of PAX3-FOXO1 activity (Fig. 1A). This approach is able to directly identify available pharmaceutical inhibitory compounds. We treated Rh4-AP2β-LF cells with 161 inhibitors (Supplementary Tab. S2) at a final concentration of 500 nM and measured cell viability as well as luciferase activity after 24 hours. Ranking compound activity according to ratio of luciferase activity over cell viability, 10 out of 161 inhibitors reduced normalized luciferase activity by at least 44% compared to untreated Rh4-AP2β-LF cells (Fig. 1D). With a normalized luciferase reduction by 76% (relative ratio 0.24), the top candidate was the PLK1 inhibitor BI 2536 (34).

To further validate BI 2536, Rh4-AP2β-LF were treated with increasing concentrations for 24 hours. This resulted in a dose dependent reduction of normalized luciferase activity with an IC_{50} of 17.40 nM (Fig 1E; $IC_{50/48h}$ =15.75 nM; $IC_{50/72h}$ =10.20 nM, Supplementary Fig. S1C). Interestingly, the median IC_{50} value of aRMS cell lines was 15.03 nM versus a median IC_{50} of 31.86 nM in eRMS cell lines (Supplementary Fig. S2A). PLK1 inhibition by BI 2536 induced apoptosis in Rh4 cells as shown by PARP cleavage (Supplementary Fig. S2B) as well as by relative increase in caspase 3/7 activity (Supplementary Fig. S2C). To demonstrate the potential relevance of PLK1 in aRMS, we analyzed the expression of PLK1 protein across a panel of eight different aRMS cell lines by immunoblotting. All of the cell lines expressed the kinase with Rh4, Rh41 and RMS13 cells displaying the highest protein levels (Fig. 1F).

In conclusion, we identified PLK1 as the most promising candidate kinase by both siRNA and small-molecule compound screen, which therefore represents a potential target for treatment of aRMS.

PLK1 inhibition reduces PAX3-FOXO1 activity

To confirm PLK1 as regulator of the fusion protein, we analyzed a panel of PAX3-FOXO1 target genes. We measured relative mRNA expression of the activated target genes AP2β, FGFR4, CDH3 and PIPOX (8, 9, 12, 13, 36-38) and the repressed differentiation marker MYL1 (39) by qRT-PCR after 48 hours of either PLK1 silencing (si1341 and siS449) or small-molecule inhibition (BI 2536 and BI 6727). In RMS13 cells, knockdown of PLK1 achieved 80% (si1341) and 82% (siS449) of silencing without affecting PAX3-FOXO1 mRNA expression. However, expression of all target genes was significantly modulated (Fig. 2A). In Rh4 cells, knockdown efficiencies by si1341 reached 86% with similar modulation of target gene expression, whereas silencing by siS449 reached 81% without significant effects on target genes (Fig. 2B). Nevertheless, treatment with both inhibitors, BI 2536 and BI 6727, significantly affected target gene expression in both cell lines.

In summary, PLK1 inhibition, either by genetic or pharmacological means, significantly altered transcription of PAX3-FOXO1 downstream targets suggesting a specific link between the kinase and the fusion protein.

PLK1 binds to and phosphorylates PAX3-FOXO1

We assessed direct interaction of PLK1 and PAX3-FOXO1 by co-immunoprecipitation of the endogenous proteins in Rh4 cells. PAX3-FOXO1 was pulled down using either anti-PAX3 or anti-FOXO1 antibody. In both cases, PLK1 was co-immunoprecipitated with the fusion protein but not with the negative control as shown by Western blot analysis (Fig. 3A). In a reciprocal approach, the kinase was pulled down by anti-PLK1 antibody and

PAX3-FOXO1 was found to co-immunoprecipitate as well (Fig. 3B). These findings indicate that PLK1 and PAX3-FOXO1 can directly interact in aRMS cells.

Furthermore, we interrogated this interaction under drug treatment conditions. Rh4 cells were transfected with FLAG-tagged PAX3-FOXO1 or FLAG-tagged GFP, which were then immunoprecipitated after DMSO or BI 2536 treatment for 16 hours using an anti-FLAG antibody. Again, we found PLK1 to interact with the fusion protein, but not with GFP (Fig. 3C). Surprisingly, interaction even increased after treatment with BI 2536, which arrested cells in G2-M (Supplementary Fig. S2D and (34, 40)). This indicates that PLK1 might control PAX3-FOXO1 mainly at the transition to mitosis.

PLK1 substrates contain the consensus motifs [D/E/N]Xp[S/T] or p[S/T]F (41) and several of these can also be found in PAX3-FOXO1 suggesting that it might be a direct target of PLK1. *In silico* analysis using GPS-Polo 1.0 (42) predicted S503 and S457 as potential phosphorylation sites with a high cut-off threshold (Fig. 3D). To directly analyze whether one of these consensus sites is phosphorylated in the fusion protein, FLAG-tagged PAX3-FOXO1 was purified from aRMS cells. Using mass spectrometry, we identified the peptide TSSNASTISGR containing S503 as one out of eleven phospho-peptides (Supplementary Tab. S3). Furthermore, applying a phospho-specific antibody to exactly localize the phosphorylated residue, we detected phosphorylation at S503+S506 (corresponding to phospho-S322+S325 in FOXO1 against which the antibody is directed) directly demonstrating that the predicted site is phosphorylated in aRMS cells (Fig. 3E).

To assess whether PLK1 can phosphorylate S503, we purified FLAG-PAX3-FOXO1 from HEK293T cells, dephosphorylated the protein by calf intestine alkaline phosphatase (CIAP) and subsequently performed *in vitro* kinase assays using recombinant PLK1. Mass spectrometry confirmed that PLK1 phosphorylated the peptide TSSNASTISGR. In total, this peptide contains six serine or threonine sites, but the data indicated that only S503 or T504 could be considered as potential phosphorylation sites (Supplementary

Fig. S3). To distinguish these two possibilities, we used the phospho-specific antibody recognizing phospho-S503+S506. Western blot analysis indeed revealed specific phosphorylation at these positions indicating that S503 is the site being phosphorylated by PLK1 (Fig. 3F).

These data suggest that PLK1 and PAX3-FOXO1 are direct interaction partners and that PLK1 can phosphorylate the fusion protein at S503.

PLK1 stabilizes PAX3-FOXO1 protein

To further explore the biological functions of this phosphorylation site, we transfected RD eRMS cells lacking endogenous PAX3-FOXO1 with plasmids expressing either PAX3-FOXO1 wild type or mutated PAX3-FOXO1-S503A. Cells were then treated with cycloheximide for 6 hours to assess protein turnover by immunoblotting and densitometric quantification. Interestingly, the mutant protein was significantly less stable than the wild type protein (protein amount reduced by 47%) (Fig. 4A and 4B).

Next, the stability of endogenous PAX3-FOXO1 upon PLK1 depletion was examined in two aRMS cell lines. Treatment with 8 nM siRNA 1341 for 48 hours reduced PLK1 protein by 43% in RMS13 cells and 53% in Rh4 cells respectively and induced a slight degradation of PAX3-FOXO1 (23% and 11%, calculated from representative blots shown in Fig. 4C). Upon silencing with the more efficient siRNA S449 (reduction of PLK1 by 94% (RMS13) and 83% (Rh4)), we observed degradation of the fusion protein by 48% and 41% compared to scrambled control treatment (Fig. 4D). These results suggest that stability of PAX3-FOXO1 is modulated by phosphorylation at S503. Indeed, inhibition of PLK1 activity by BI 2536 (15 nM) and BI 6727 (20 nM) led to similar reduction of PAX3-FOXO1 protein levels (53% and 64% in RMS13, 44% and 49% in Rh4 cells) (Fig. 4E). In addition, increased ubiquitination of PAX3-FOXO1 upon PLK1 inhibition confirmed its proteasomal degradation (Fig. 4F), which moreover, could be rescued by adding low

concentrations of the proteasomal inhibitor Bortezomib (43) in a dose dependent manner (Fig. 4G).

In conclusion, these experiments imply that PLK1-mediated phosphorylation at S503 protects PAX3-FOXO1 from ubiquitination and consequent proteasomal degradation and thus maintains the transcriptional activity of the fusion protein.

PLK1 inhibition causes tumor regression in xenografts

Based on our *in vitro* results, we further validated PLK1 as an *in vivo* target using xenograft mouse models. Immunocompromised NOD/Scid il2rg$^{-/-}$ (NSG) mice were engrafted subcutaneously with Rh4, Rh4luc and RMS13luc cells expressing luciferase for *in vivo* imaging. Mice with established tumors of varying sizes (65 mm^3 – 470 mm^3) were treated intravenously with vehicle or BI 2536 at a dose of 40 mg/kg for three weeks on two consecutive days per week (34). Every treatment group of three to five mice included two mice with large tumors of at least 300 mm^3. Absolute tumor volumes measured by caliper in mice bearing Rh4 tumors revealed a complete tumor regression upon BI 2536 treatment in all mice, even when the starting volume was as high as 370 mm^3 (Fig. 5A). Similarly, luciferase activity was reduced in both cell lines by close to 100% (Fig. 5A and 5B). Tumors of additional mice were treated for two cycles only, isolated after a two-week recovery phase, paraffin-embedded, and immunohistochemically stained. Vehicle treated tumors showed highly cellular histology with strong expression of Myogenin and AP2β consistent with aRMS. In contrast, treated xenografts displayed a high degree of necrotic areas and fibrosis. Importantly, expression of PAX3-FOXO1 target genes AP2β and P-Cadherin (CDH3) was significantly lower compared to untreated xenografts.

These data impressively illustrate that PLK1 activity plays a major role in aRMS tumor cell survival corroborating our *in vitro* results. Therefore, PLK1 inhibitors such as BI 2536 might represent very potent novel treatment options for aRMS.

PLK1 is overexpressed in human tumor biopsies and correlates with PAX3-FOXO1 activity and survival

To ensure that our findings are not restricted to aRMS cell lines, PLK1 expression was analyzed in patient tumor biopsies. We utilized PLK mRNA expression data of PAX3-FOXO1 positive aRMS tumors from two independent data sets (9, 13) and compared them to PLK expression in normal muscle tissue (44). We found that mRNA levels of PLK1 and PLK4, but not PLK2 and PLK3, were significantly higher in tumor samples than in normal muscle biopsies (Fig. 6A and Supplementary Fig. S4).

To validate PLK1 as a clinically relevant therapeutic target, we immunohistochemically stained a tissue microarray including tumor biopsies of 49 aRMS patients. Tumors were divided into high and low expressing subgroups as described in Material and Methods (Fig. 6B). To correlate PAX3-FOXO1 activity with PLK1 expression *in vivo*, we assessed in parallel expression of the PAX3-FOXO1 target gene AP2β. In a majority of tumors (34 out of 45), AP2β staining from the same tumor significantly correlated with expression of PLK1 (Pearson correlation p-value: 0.0004, Fig. 6C). This was not the case for co-staining with the proliferation marker MIB1 (Supplementary Fig. S5). These results support our previous findings and a mechanism whereby activity of PAX3-FOXO1 is modulated by PLK1.

Importantly, outcome as measured for event free (EFS) and overall survival (OS) by Kaplan-Meier analysis was significantly worse for patients with high PLK1 expression (Fig. 6D). Five-year survival rates for patients in the PLK1 high expression cohort were only 15.4% (EFS) and 20.2% (OS). Therefore, the hazard ratio for events was 2.3 times higher (Wald test: $p = 0.019$) and for death even 3.16 times higher (Wald test: $p = 0.004$) for patients with high PLK1 expression. Moreover, multivariate analyses including the factors age, sex and tumor localization identified PLK1 status as the only significant risk associated variable (Tab. 1). The very dismal survival rates for the high expression

cohort emphasize the importance of PLK1 expression and suggest that PLK1 is a prognostic risk factor for fusion-positive RMS.

In summary, our results imply that PLK1 is a highly attractive target for the treatment of aggressive aRMS, which warrants further investigations in clinical studies.

Discussion

This study describes a novel PLK1 - PAX3-FOXO1 oncogenic axis in aRMS. We show modulation of PAX3-FOXO1 activity by PLK1 based on direct protein-protein interaction and phosphorylation at S503 leading to stabilization of the fusion protein. In addition, *in vivo* treatment with PLK1 inhibitor demonstrated tumor regression and immunohistochemical analysis of PLK1 protein expression in human biopsies revealed its novel prognostic impact.

To improve previous screenings for targets in aRMS, which concentrated mainly on cell viability (45), we focused on transcriptional activity of PAX3-FOXO1 by employing aRMS (Rh4) cells stably expressing an AP2β-promoter reporter construct. Using the ratio of reporter activity versus cell viability, we were able to exclude generally cytotoxic drugs. Strikingly, a kinome-wide siRNA as well as a small-molecule library screen identified PLK1 as top hit. KEGG pathway analysis (string-db.org) showed that several additional candidates are associated with MAPK or phosphatidylinositol signaling, both of which have been previously reported in RMS (27).

To confirm PLK1 as an upstream modulator of PAX3-FOXO1 activity, we assessed expression of known endogenous PAX3-FOXO1 target genes (AP2β, FGFR4, CDH3, PIPOX and MYL1) upon inhibition by two drugs as well as by two different siRNAs in two aRMS cell lines. We observed significant target gene modulation with the exception of one siRNA in Rh4 cells. It is likely that the lack of activity might be due to compensatory effects by other members of the PLK family since BI 2536 and BI 6727 are known to affect the activities of PLK2, PLK3 and potentially PLK4 (34, 46). Indeed, next

to PLK1 also PLK4 is overexpressed in aRMS biopsies compared to normal muscle and, although not identified in the primary screen, its depletion reduced target gene expression in Rh4 cells suggesting overlapping functions of PLK1 and PLK4 (Supplementary Fig. S6). Nevertheless, our findings support the conclusion that PLK1 regulates PAX3-FOXO1 activity.

To further sustain this notion, we demonstrated direct protein-protein interaction of the endogenous proteins by co-immunoprecipitations in aRMS cells. Also, recombinant PLK1 phosphorylated the fusion protein at S503 in *in vitro* kinase assays. This residue is located within a very conserved domain in the FOXO1 part of the fusion protein and the corresponding serine in wild type FOXO1 (S322) is a site known to be phosphorylated by recombinant CK1 (47). A recent study demonstrated that wild type FOXO1 interacts with and is phosphorylated also by PLK1 during G2-M (48). Similarly, we observed enhanced interaction in this cell cycle phase. However, phosphorylation of wild type FOXO1 triggers nuclear export (47, 48), whereas PAX3-FOXO1 is located exclusively in the nucleus (22) (and own observations). Hence, phosphorylation of S503 by PLK1 must have different consequences. In fact, we observed faster degradation of PAX3-FOXO1-S503A compared to wild type after cycloheximide block due to enhanced ubiquitination upon PLK1 inhibition. It has previously also been shown that PAX3-FOXO1 has increased post-translational stability compared to wild type proteins (21). Our results are furthermore in line with studies demonstrating PLK1 to mediate stabilization of transcription factors such as the oncogene MYC (49). Interestingly, we found the fusion target gene NMYC to be degraded upon PLK1 inhibition, either by a direct or indirect mechanism (Supplementary Fig. S7), which might further sensitize aRMS as well as other NMYC expressing tumors to PLK1 inhibitors. In accordance with the proposed function of PAX3-FOXO1 in checkpoint adaptation (50), PLK1 might prevent premature degradation of PAX3-FOXO1 during the transition phase. In summary, this suggests a model whereby PLK1 phosphorylation can stabilize PAX3-FOXO1, mainly during G2-M

transition, whereas at the same time it would inhibit the wild type tumor suppressor FOXO1 to ensure cell cycle progression and survival.

We observed an almost complete tumor regression *in vivo* upon treatment with BI 2536 in two different aRMS cell lines. This is in agreement with an objective response demonstrated for the Rh30r aRMS xenograft by the Pediatric Preclinical Testing Program (51). This particular xenograft was derived from a patient that had failed prior therapies suggesting that PLK1 expression might be of prognostic relevance. Indeed, expression of PLK1 in 49 aRMS tumor biopsies significantly predicted poor prognosis for event free and overall survival. To our knowledge, PLK1 expression is therefore one of the first predictive markers next to EPHB4 that is able to stratify patients within the group of fusion-positive tumors (52).

Summarizing, our data suggest that PLK1 is a highly relevant clinical target in aRMS with several PLK1 inhibitors already in clinical development. Since it has been shown that mice can tolerate higher systemic exposure to PLK1 inhibitors than humans (51), it is likely that combination therapies need to be developed to overcome this obstacle. Nevertheless, this study reveals an important new role for PLK1 in aRMS biology apart from its known function in cell cycle that might explain increased sensitivity. Hence, our results should be directly translatable to clinical studies.

Acknowledgements

We would like to thank Stefano Ferrari for useful discussion of the project and Sabrina Steiert for her support.

References

1. Breneman JC, Lyden E, Pappo AS, Link MP, Anderson JR, Parham DM, et al. Prognostic factors and clinical outcomes in children and adolescents with metastatic rhabdomyosarcoma--a report from the Intergroup Rhabdomyosarcoma Study IV. J Clin Oncol 2003; 21: 78-84.
2. Vogelstein B, Papadopoulos N, Velculescu VE, Zhou S, Diaz LA, Jr., Kinzler KW. Cancer genome landscapes. Science 2013; 339: 1546-58.
3. Chen X, Stewart E, Shelat AA, Qu C, Bahrami A, Hatley M, et al. Targeting oxidative stress in embryonal rhabdomyosarcoma. Cancer Cell 2013; 24: 710-24.
4. Shern JF, Chen L, Chmielecki J, Wei JS, Patidar R, Rosenberg M, et al. Comprehensive Genomic Analysis of Rhabdomyosarcoma Reveals a Landscape of Alterations Affecting a Common Genetic Axis in Fusion-Positive and Fusion-Negative Tumors. Cancer Discov 2014.
5. Sorensen PH, Lynch JC, Qualman SJ, Tirabosco R, Lim JF, Maurer HM, et al. PAX3-FKHR and PAX7-FKHR gene fusions are prognostic indicators in alveolar rhabdomyosarcoma: a report from the children's oncology group. J Clin Oncol 2002; 20: 2672-9.
6. Linardic CM. PAX3-FOXO1 fusion gene in rhabdomyosarcoma. Cancer Lett 2008; 270: 10-8.
7. Olanich ME, Barr FG. A call to ARMS: targeting the PAX3-FOXO1 gene in alveolar rhabdomyosarcoma. Expert Opin Ther Targets 2013; 17: 607-23.
8. Cao L, Yu Y, Bilke S, Walker RL, Mayeenuddin LH, Azorsa DO, et al. Genome-wide identification of PAX3-FKHR binding sites in rhabdomyosarcoma reveals candidate target genes important for development and cancer. Cancer Res 2010; 70: 6497-508.
9. Davicioni E, Finckenstein FG, Shahbazian V, Buckley JD, Triche TJ, Anderson MJ. Identification of a PAX-FKHR gene expression signature that defines molecular classes and determines the prognosis of alveolar rhabdomyosarcomas. Cancer Res 2006; 66: 6936-46.
10. Ebauer M, Wachtel M, Niggli FK, Schafer BW. Comparative expression profiling identifies an in vivo target gene signature with TFAP2B as a mediator of the survival function of PAX3/FKHR. Oncogene 2007; 26: 7267-81.
11. Khan J, Simon R, Bittner M, Chen Y, Leighton SB, Pohida T, et al. Gene expression profiling of alveolar rhabdomyosarcoma with cDNA microarrays. Cancer Res 1998; 58: 5009-13.
12. Lae M, Ahn EH, Mercado GE, Chuai S, Edgar M, Pawel BR, et al. Global gene expression profiling of PAX-FKHR fusion-positive alveolar and PAX-FKHR fusion-negative embryonal rhabdomyosarcomas. J Pathol 2007; 212: 143-51.
13. Wachtel M, Dettling M, Koscielniak E, Stegmaier S, Treuner J, Simon-Klingenstein K, et al. Gene expression signatures identify rhabdomyosarcoma subtypes and detect a novel t(2;2)(q35;p23) translocation fusing PAX3 to NCOA1. Cancer Res 2004; 64: 5539-45.
14. Bernasconi M, Remppis A, Fredericks WJ, Rauscher FJ, 3rd, Schafer BW. Induction of apoptosis in rhabdomyosarcoma cells through down-regulation of PAX proteins. Proc Natl Acad Sci U S A 1996; 93: 13164-9.
15. Ayyanathan K, Fredericks WJ, Berking C, Herlyn M, Balakrishnan C, Gunther E, et al. Hormone-dependent tumor regression in vivo by an inducible transcriptional repressor directed at the PAX3-FKHR oncogene. Cancer Res 2000; 60: 5803-14.
16. Stegmaier S, Poremba C, Schaefer KL, Leuschner I, Kazanowska B, Bekassy AN, et al. Prognostic value of PAX-FKHR fusion status in alveolar rhabdomyosarcoma: a report

from the cooperative soft tissue sarcoma study group (CWS). Pediatr Blood Cancer 2011; 57: 406-14.
17. Missiaglia E, Williamson D, Chisholm J, Wirapati P, Pierron G, Petel F, et al. PAX3/FOXO1 fusion gene status is the key prognostic molecular marker in rhabdomyosarcoma and significantly improves current risk stratification. J Clin Oncol 2012; 30: 1670-7.
18. Davis RJ, Barr FG. Fusion genes resulting from alternative chromosomal translocations are overexpressed by gene-specific mechanisms in alveolar rhabdomyosarcoma. Proc Natl Acad Sci U S A 1997; 94: 8047-51.
19. Bennicelli JL, Edwards RH, Barr FG. Mechanism for transcriptional gain of function resulting from chromosomal translocation in alveolar rhabdomyosarcoma. Proc Natl Acad Sci U S A 1996; 93: 5455-9.
20. Bennicelli JL, Advani S, Schafer BW, Barr FG. PAX3 and PAX7 exhibit conserved cis-acting transcription repression domains and utilize a common gain of function mechanism in alveolar rhabdomyosarcoma. Oncogene 1999; 18: 4348-56.
21. Miller PJ, Hollenbach AD. The oncogenic fusion protein Pax3-FKHR has a greater post-translational stability relative to Pax3 during early myogenesis. Biochim Biophys Acta 2007; 1770: 1450-8.
22. del Peso L, Gonzalez VM, Hernandez R, Barr FG, Nunez G. Regulation of the forkhead transcription factor FKHR, but not the PAX3-FKHR fusion protein, by the serine/threonine kinase Akt. Oncogene 1999; 18: 7328-33.
23. Amstutz R, Wachtel M, Troxler H, Kleinert P, Ebauer M, Haneke T, et al. Phosphorylation regulates transcriptional activity of PAX3/FKHR and reveals novel therapeutic possibilities. Cancer Res 2008; 68: 3767-76.
24. Liu L, Wu J, Ong SS, Chen T. Cyclin-dependent kinase 4 phosphorylates and positively regulates PAX3-FOXO1 in human alveolar rhabdomyosarcoma cells. PLoS One 2013; 8: e58193.
25. Jothi M, Mal M, Keller C, Mal AK. Small Molecule Inhibition of PAX3-FOXO1 through AKT Activation Suppresses Malignant Phenotypes of Alveolar Rhabdomyosarcoma. Mol Cancer Ther 2013.
26. Strebhardt K, Ullrich A. Targeting polo-like kinase 1 for cancer therapy. Nat Rev Cancer 2006; 6: 321-30.
27. Holtrich U, Wolf G, Brauninger A, Karn T, Bohme B, Rubsamen-Waigmann H, et al. Induction and down-regulation of PLK, a human serine/threonine kinase expressed in proliferating cells and tumors. Proc Natl Acad Sci U S A 1994; 91: 1736-40.
28. Cholewa BD, Liu X, Ahmad N. The Role of Polo-like Kinase 1 in Carcinogenesis: Cause or Consequence? Cancer Res 2013.
29. Guenther MK, Graab U, Fulda S. Synthetic lethal interaction between PI3K/Akt/mTOR and Ras/MEK/ERK pathway inhibition in rhabdomyosarcoma. Cancer Lett 2013; 337: 200-9.
30. Renshaw J, Taylor KR, Bishop R, Valenti M, De Haven Brandon A, Gowan S, et al. Dual Blockade of the PI3K/AKT/mTOR (AZD8055) and RAS/MEK/ERK (AZD6244) Pathways Synergistically Inhibits Rhabdomyosarcoma Cell Growth In Vitro and In Vivo. Clin Cancer Res 2013; 19: 5940-51.
31. Scholl FA, Betts DR, Niggli FK, Schafer BW. Molecular features of a human rhabdomyosarcoma cell line with spontaneous metastatic progression. Br J Cancer 2000; 82: 1239-45.
32. Hinson AR, Jones R, Crose LE, Belyea BC, Barr FG, Linardic CM. Human rhabdomyosarcoma cell lines for rhabdomyosarcoma research: utility and pitfalls. Front Oncol 2013; 3: 183.
33. Kikuchi K, Tsuchiya K, Otabe O, Gotoh T, Tamura S, Katsumi Y, et al. Effects of PAX3-FKHR on malignant phenotypes in alveolar rhabdomyosarcoma. Biochem Biophys Res Commun 2008; 365: 568-74.

34. Steegmaier M, Hoffmann M, Baum A, Lenart P, Petronczki M, Krssak M, et al. BI 2536, a potent and selective inhibitor of polo-like kinase 1, inhibits tumor growth in vivo. Curr Biol 2007; 17: 316-22.
35. Grass B, Wachtel M, Behnke S, Leuschner I, Niggli FK, Schafer BW. Immunohistochemical detection of EGFR, fibrillin-2, P-cadherin and AP2beta as biomarkers for rhabdomyosarcoma diagnostics. Histopathology 2009; 54: 873-9.
36. Wachtel M, Runge T, Leuschner I, Stegmaier S, Koscielniak E, Treuner J, et al. Subtype and prognostic classification of rhabdomyosarcoma by immunohistochemistry. J Clin Oncol 2006; 24: 816-22.
37. Marshall AD, van der Ent MA, Grosveld GC. PAX3-FOXO1 and FGFR4 in alveolar rhabdomyosarcoma. Mol Carcinog 2012; 51: 807-15.
38. Thuault S, Hayashi S, Lagirand-Cantaloube J, Plutoni C, Comunale F, Delattre O, et al. P-cadherin is a direct PAX3-FOXO1A target involved in alveolar rhabdomyosarcoma aggressiveness. Oncogene 2013; 32: 1876-87.
39. De Pitta C, Tombolan L, Albiero G, Sartori F, Romualdi C, Jurman G, et al. Gene expression profiling identifies potential relevant genes in alveolar rhabdomyosarcoma pathogenesis and discriminates PAX3-FKHR positive and negative tumors. Int J Cancer 2006; 118: 2772-81.
40. Lenart P, Petronczki M, Steegmaier M, Di Fiore B, Lipp JJ, Hoffmann M, et al. The small-molecule inhibitor BI 2536 reveals novel insights into mitotic roles of polo-like kinase 1. Curr Biol 2007; 17: 304-15.
41. Kettenbach AN, Wang T, Faherty BK, Madden DR, Knapp S, Bailey-Kellogg C, et al. Rapid determination of multiple linear kinase substrate motifs by mass spectrometry. Chem Biol 2012; 19: 608-18.
42. Liu Z, Ren J, Cao J, He J, Yao X, Jin C, et al. Systematic analysis of the Plk-mediated phosphoregulation in eukaryotes. Brief Bioinform 2013; 14: 344-60.
43. Adams J, Palombella VJ, Sausville EA, Johnson J, Destree A, Lazarus DD, et al. Proteasome inhibitors: a novel class of potent and effective antitumor agents. Cancer Res 1999; 59: 2615-22.
44. Bakay M, Wang Z, Melcon G, Schiltz L, Xuan J, Zhao P, et al. Nuclear envelope dystrophies show a transcriptional fingerprint suggesting disruption of Rb-MyoD pathways in muscle regeneration. Brain 2006; 129: 996-1013.
45. Hu K, Lee C, Qiu D, Fotovati A, Davies A, Abu-Ali S, et al. Small interfering RNA library screen of human kinases and phosphatases identifies polo-like kinase 1 as a promising new target for the treatment of pediatric rhabdomyosarcomas. Mol Cancer Ther 2009; 8: 3024-35.
46. Rudolph D, Steegmaier M, Hoffmann M, Grauert M, Baum A, Quant J, et al. BI 6727, a Polo-like kinase inhibitor with improved pharmacokinetic profile and broad antitumor activity. Clin Cancer Res 2009; 15: 3094-102.
47. Rena G, Woods YL, Prescott AR, Peggie M, Unterman TG, Williams MR, et al. Two novel phosphorylation sites on FKHR that are critical for its nuclear exclusion. Embo J 2002; 21: 2263-71.
48. Yuan C, Wang L, Zhou L, Fu Z. The function of FOXO1 in the late phases of the cell cycle is suppressed by PLK1-mediated phosphorylation. Cell Cycle 2014; 13.
49. Tan J, Li Z, Lee PL, Guan P, Aau MY, Lee ST, et al. PDK1 signaling toward PLK1-MYC activation confers oncogenic transformation, tumor-initiating cell activation, and resistance to mTOR-targeted therapy. Cancer Discov 2013; 3: 1156-71.
50. Kikuchi K, Hettmer S, Aslam MI, Michalek JE, Laub W, Wilky BA, et al. Cell-cycle dependent expression of a translocation-mediated fusion oncogene mediates checkpoint adaptation in rhabdomyosarcoma. PLoS Genet 2014; 10: e1004107.
51. Gorlick R, Kolb EA, Keir ST, Maris JM, Reynolds CP, Kang MH, et al. Initial testing (stage 1) of the polo-like kinase inhibitor volasertib (BI 6727), by the Pediatric Preclinical Testing Program. Pediatr Blood Cancer 2014; 61: 158-64.

52. Aslam MI, Abraham J, Mansoor A, Druker BJ, Tyner JW, Keller C. PDGFRbeta reverses EphB4 signaling in alveolar rhabdomyosarcoma. Proc Natl Acad Sci U S A 2014; 111: 6383-8.

Figure Legends

Figure 1. siRNA and drug screening identify PLK1 as regulator of PAX3-FOXO1

(A) Schematic representation of screening strategy. PAX3-FOXO1 is phosphorylated, transcriptionally active and induces expression of the luciferase gene, which is under the control of the PAX3-FOXO1-responsive AP2β promoter. Kinase silencing and small-molecule inhibition reduce PAX3-FOXO1 transcriptional activity and result in a decreased expression of the luciferase gene.

(B) Results of kinome-wide siRNA screen. RNA silencing was carried out for 48h using 50 nM siRNA. The luciferase readout was normalized to cell viability measured by WST-1 assay. siRNAs targeting luciferase (pGL4) and PAX3-FOXO1 served as positive controls for reduced activity/cell viability ratio (LF/V) and siKIF11 for reduced cell viability. Reduced LF/V ratio upon PLK1 silencing is marked in black. *Data points*, mean of three independent experiments performed in triplicates; *threshold*, 1.5 SDs of mean of luciferase knockdown

(C) Sub-screen of candidate kinases. RNA silencing was carried out in Rh4 and RMS13 cells for 72h using 50 nM siRNA. Cell viability was measured by WST-1 assay and set relative to scrambled knockdown. *Data points*, mean of three independent experiments performed in triplicates; Student's t-test for PLK1 knockdown *** $p < 0.001$, ** $p < 0.01$

(D) Illustration of the ten most effective drugs. Rh4-AP2β-LF cells were treated with a small-molecule compound library at a final concentration of 500 nM for 24h and luciferase activity (LF) and cell viability (V) were measured. Relative values compared to untreated cells as well as the resulting LF/V ratios are shown. *Columns*, mean of technical triplicates; *bars,* SD

(E) Drug response curve of BI 2536 based on LF/V ratio. Rh4-AP2β-LF cells were treated with increasing concentrations of BI 2536 for 24h. LF/V values were measured relative to untreated cells. *Data points,* mean of technical triplicates; non-linear regression curve fitting using Prism GraphPad

(F) PLK1 expression in aRMS cell lines shown by Western blot analysis

Figure 2. PLK1 silencing and inhibition reduce PAX3-FOXO1 activity

Relative mRNA expression of PAX3-FOXO1 and its target genes upon PLK1 knockdown and inhibition. C_T values relative to scrambled knockdown or DMSO treatment were measured by qRT-PCR and normalized to GAPDH expression.

(A and B) PLK1 was silenced for 48h using two different sequences (25 nM si1341 and 8 nM siS449) in RMS13 and Rh4 cells.

(C and D) RMS13 and Rh4 cells were treated with 15 nM BI 2536 or 20 nM BI 6727 for 48h.

Columns, geometric mean of at least 4 independent experiments performed in triplicates; *bars,* 95% confidence interval; * significant according to 95% CI

Figure 3. PLK1 phosphorylates PAX3-FOXO1

(A) Western blot analysis showing endogenous Co-IP of PLK1 after PAX3-FOXO1 immunoprecipitation in Rh4 cells. Beads-only were used as negative control.

(B) Western blot analysis showing endogenous Co-IP of PAX3-FOXO1 after PLK1 immunoprecipitation in Rh4 cells. Beads-only were used as negative control.

(C) Western blot analysis of PLK1 after FLAG immunoprecipitation from Rh4 cells expressing FLAG-PAX3-FOXO1. Cells were treated with DMSO or 15 nM BI 2536 for 16h. FLAG-GFP was used as negative control.

(D) *In silico* analysis using the phospho-site prediction software GPS-Polo 1.0 for phosphorylation of PAX3-FOXO1 by PLK

(E) Western blot analysis of FLAG-PAX3-FOXO1 purified from Rh4 cells using anti phospho-S503+S506 antibody

(F) PLK1 *in vitro* kinase assay. HEK293T cells were transfected by FLAG-PAX3-FOXO1 expressing plasmid, purified, dephosphorylated by CIAP and re-phosphorylated by

recombinant PLK1. Phospho-peptide identified by mass spectrometric analysis and Western blot analysis using anti phospho-S503+S506 antibody are shown.

Figure 4. PLK1 stabilizes PAX3-FOXO1

(A) Western blot analysis of exogenous, wild type or phospho-mutant PAX3-FOXO1 degradation. RD cells were transfected with PAX3-FOXO1 wild type or PAX3-FOXO1-S503A expressing constructs and treated for 6h with DMSO or 35 μM cycloheximide (CHX).

(B) Quantification of exogenous PAX3-FOXO1 degradation by densitometry. Levels were normalized to GAPDH. *Columns,* mean of three independent experiments; *bars,* SD; Student's t-test ** p= 0.0052

(C and D) Western blot analysis of endogenous PAX3-FOXO1 degradation upon PLK1 silencing. RMS13 and Rh4 cells were transfected with 25 nM si1341 or 8 nM siS449 for 48h.

(E) Western blot analysis of endogenous PAX3-FOXO1 degradation upon PLK1 inhibition. RMS13 and Rh4 cells were treated with DMSO, 15 nM BI 2536 or 20 nM BI 6727 for 48h.

(F) Ubiquitination studies. Western blot analysis after FLAG immunoprecipitation from Rh4 cells expressing FLAG-PAX3-FOXO1 and HA-Ubiquitin. Cells were treated with DMSO, 200 nM BI2536 or 200 nM BI6727 for 21h prior to addition of 10 μM MG-132 for 5h.

(G) Western blot analysis showing rescue of endogenous PAX3-FOXO1 degradation by the proteasomal inhibitor Bortezomib. Rh4 cells were treated with 15 nM BI 2536 for 20h. Bortezomib was simultaneously titrated to the cells. Densitometric quantification normalized to β-Tubulin is indicated.

Figure 5. PLK1 inhibition causes tumor regression *in vivo*

In vivo drug treatment of NOD/Scid il2rg$^{-/-}$ mice engrafted with Rh4 (n=10), Rh4luc (n=6) and RMS13luc (n=6) (luc = luciferase expressing). Mice bearing established tumors were treated intravenously for three cycles with either vehicle control or BI 2536 at a dose of 40 mg/kg twice weekly on two consecutive days (indicated by triangles).

(A) Absolute and relative tumor volumes upon treatment. Absolute tumor volume was measured by caliper (upper two panels). *In vivo* imaging was performed for luciferase expressing tumors. Relative bioluminescence (photons/second) is depicted (lower four panels).

(B) Illustration of tumor regression by picture series during treatment phase of two representative mice

(C) Immunohistochemistry of a control and a BI 2536 treated tumor. Rh4luc tumors were treated for two cycles with either vehicle control or BI 2536 at a dose of 40 mg/kg. Tumors were excised two weeks after the end of treatment and immunohistochemically stained.

Figure 6. PLK1 is an overexpressed, prognostic marker that correlates with PAX3-FOXO1 activity in tumor biopsies

(A) PLK1 gene expression in normal human muscle (n=121) and in PAX3-FOXO1 positive aRMS patient-derived biopsies (n=46) measured by microarray (Affymetrix HG-U133A). *Box plot,* minimum to maximum; Student's t-test $p < 0.0001$

(B) Patient-derived tissue microarray immunohistochemically stained for PLK1 (n=49) and AP2β (n=45) expression. Patients were grouped according to high (n=26) and low (n=23) PLK1 expression and high (n=28) and low AP2β (n=17) expression. Representative tumor of PLK1 high expression cohort and a tumor with very low expression are shown next to AP2β staining of the same tumor.

(C) Pearson correlation of PLK1 and AP2β expression based on tissue microarray

(n=45); p= 0.0004

(D) Kaplan-Maier survival curves of PLK1 low and high expression cohorts based on tissue microarray. Log-rank test

Figure 1

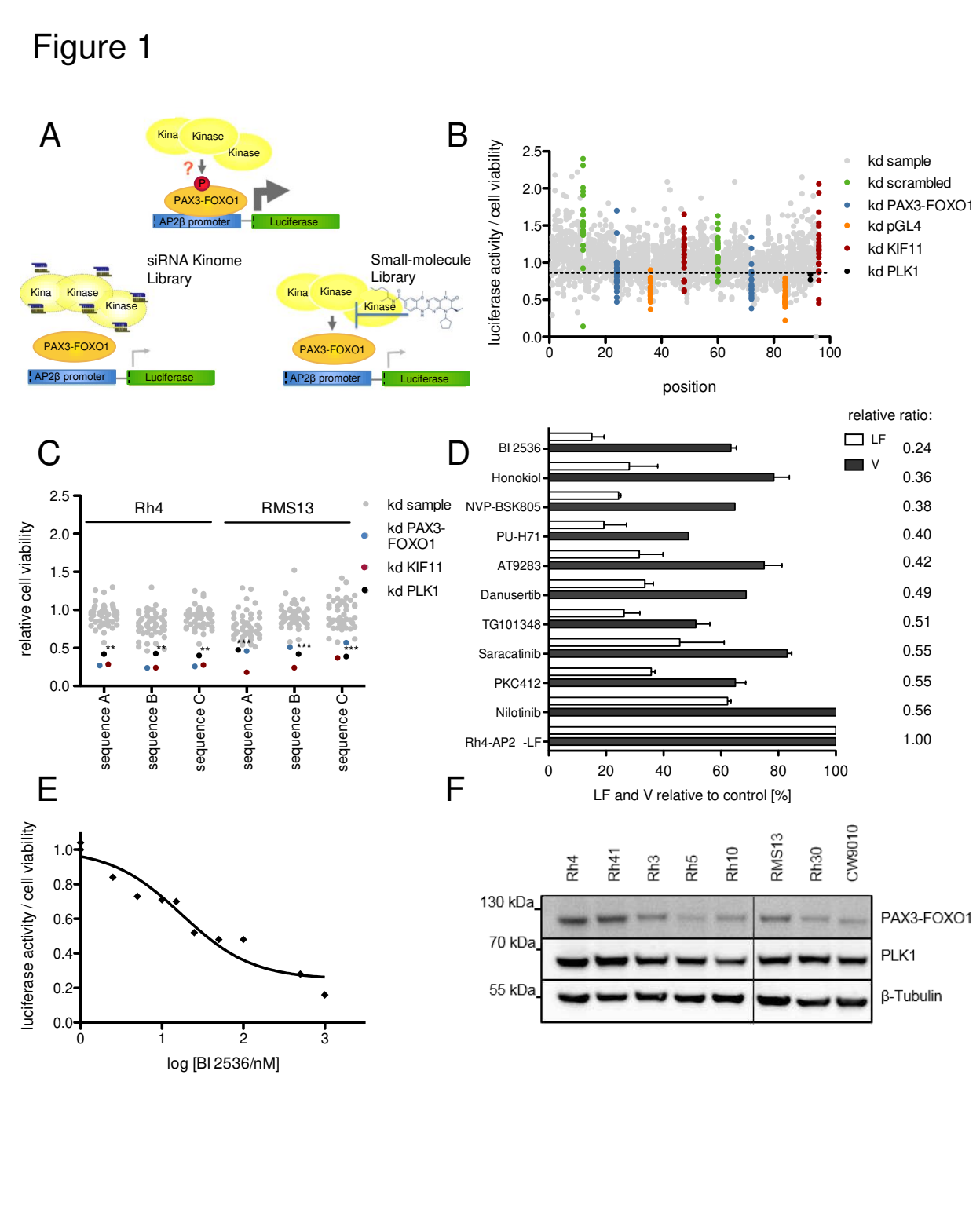
A
Kina
Kinase
Kinase
?
P
PAX3-FOXO1
AP2β promoter
Luciferase
siRNA Kinome Library
Small-molecule Library
B
luciferase activity / cell viability
position
kd sample
kd scrambled
kd PAX3-FOXO1
kd pGL4
kd KIF11
kd PLK1
C
Rh4
RMS13
relative cell viability
sequence A
sequence B
sequence C
D
relative ratio:
LF
V
BI 2536
Honokiol
NVP-BSK805
PU-H71
AT9283
Danusertib
TG101348
Saracatinib
PKC412
Nilotinib
Rh4-AP2 -LF
0.24
0.36
0.38
0.40
0.42
0.49
0.51
0.55
0.55
0.56
1.00
LF and V relative to control [%]
E
luciferase activity / cell viability
log [BI 2536/nM]
F
Rh4
Rh41
Rh3
Rh5
Rh10
RMS13
Rh30
CW9010
130 kDa
70 kDa
55 kDa
PAX3-FOXO1
PLK1
β-Tubulin

Figure 2

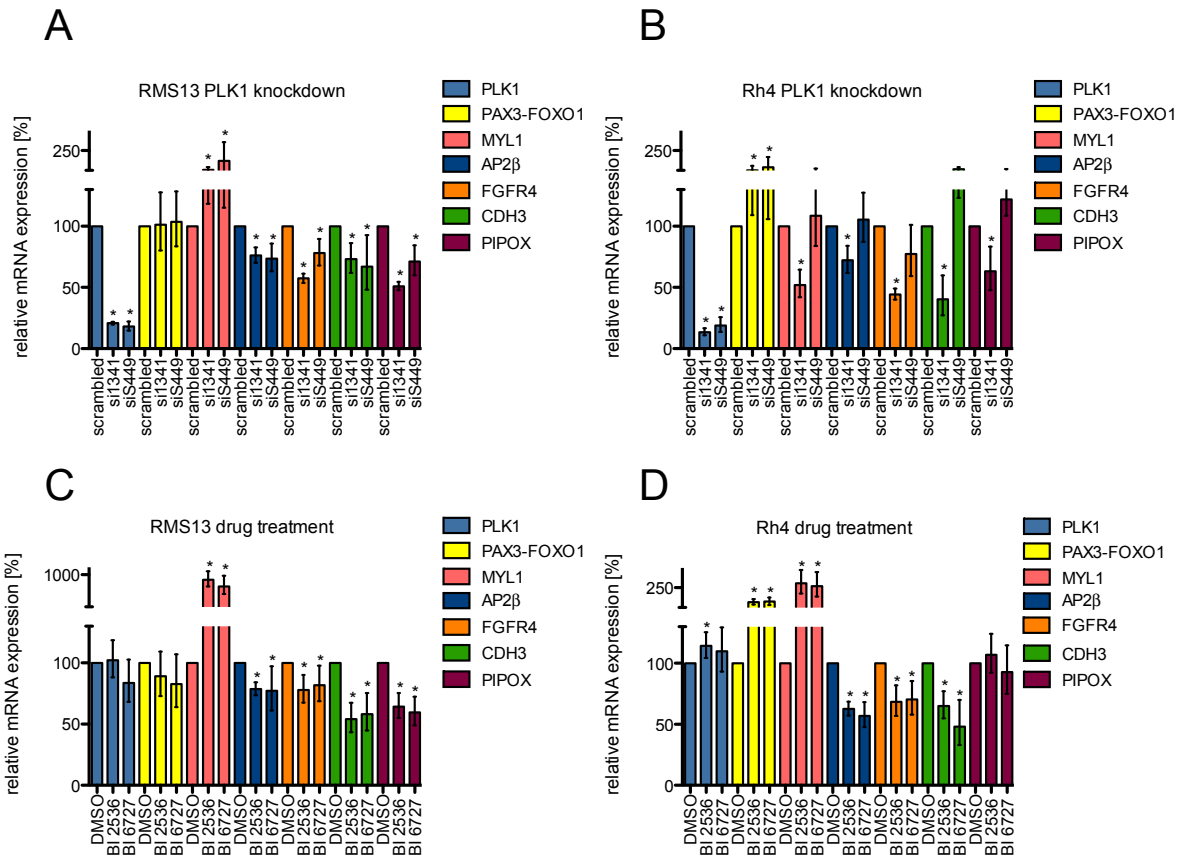
A
RMS13 PLK1 knockdown
relative mRNA expression [%]
0
50
100
250
scrambled
si1341
siS449
B
Rh4 PLK1 knockdown
C
RMS13 drug treatment
1000
DMSO
BI 2536
BI 6727
D
Rh4 drug treatment
PLK1
PAX3-FOXO1
MYL1
AP2β
FGFR4
CDH3
PIPOX

Figure 3

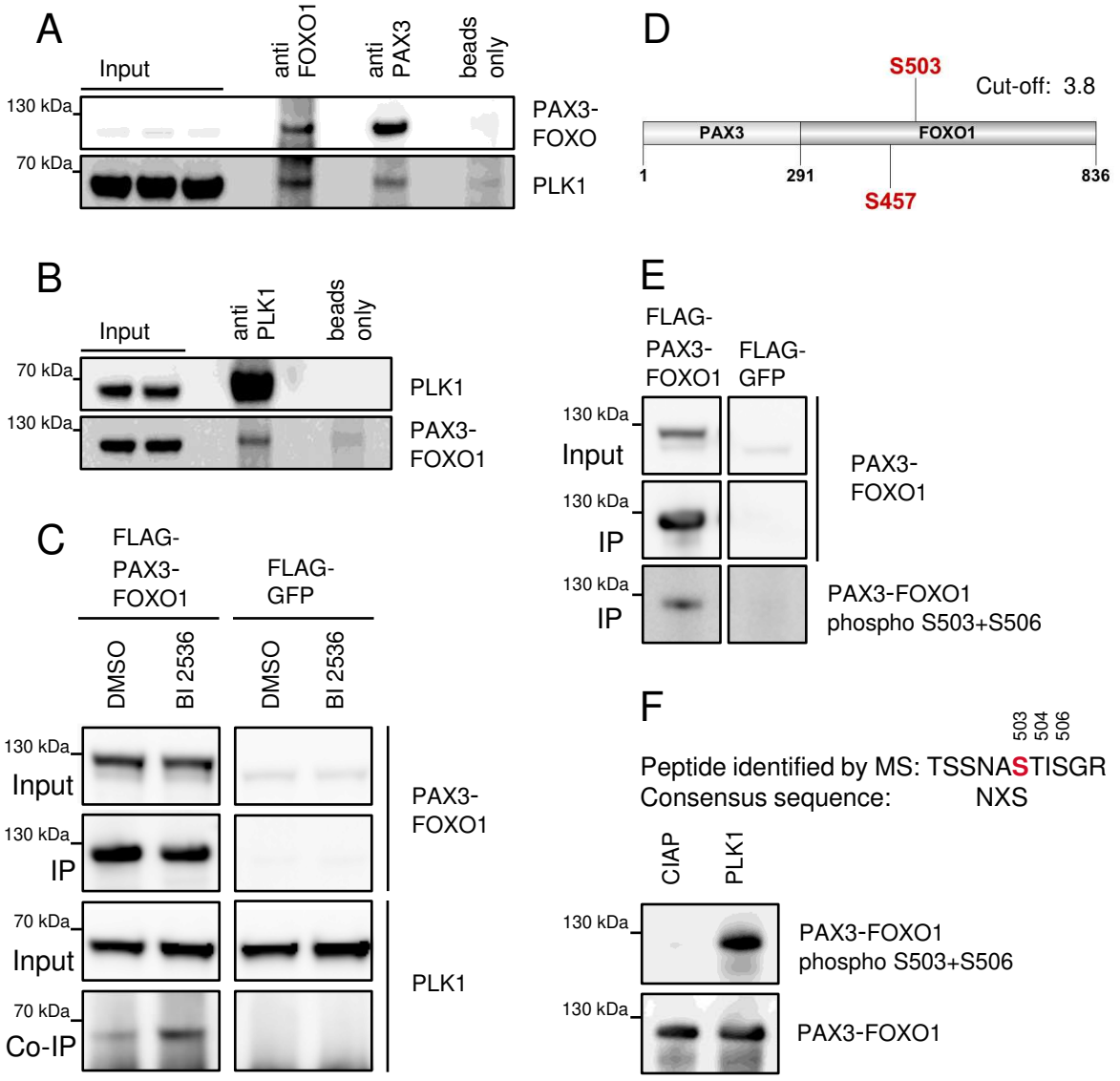
A
Input
anti FOXO1
anti PAX3
beads only
130 kDa
70 kDa
PAX3-FOXO
PLK1
B
Input
anti PLK1
beads only
70 kDa
130 kDa
PLK1
PAX3-FOXO1
C
FLAG-PAX3-FOXO1
FLAG-GFP
DMSO
BI 2536
DMSO
BI 2536
130 kDa
Input
130 kDa
IP
PAX3-FOXO1
70 kDa
Input
70 kDa
Co-IP
PLK1
D
S503
Cut-off: 3.8
PAX3
FOXO1
1
291
836
S457
E
FLAG-PAX3-FOXO1
FLAG-GFP
130 kDa
Input
130 kDa
IP
PAX3-FOXO1
130 kDa
IP
PAX3-FOXO1 phospho S503+S506
F
503 504 506
Peptide identified by MS: TSSNASTISGR
Consensus sequence: NXS
CIAP
PLK1
130 kDa
PAX3-FOXO1 phospho S503+S506
130 kDa
PAX3-FOXO1

Figure 4

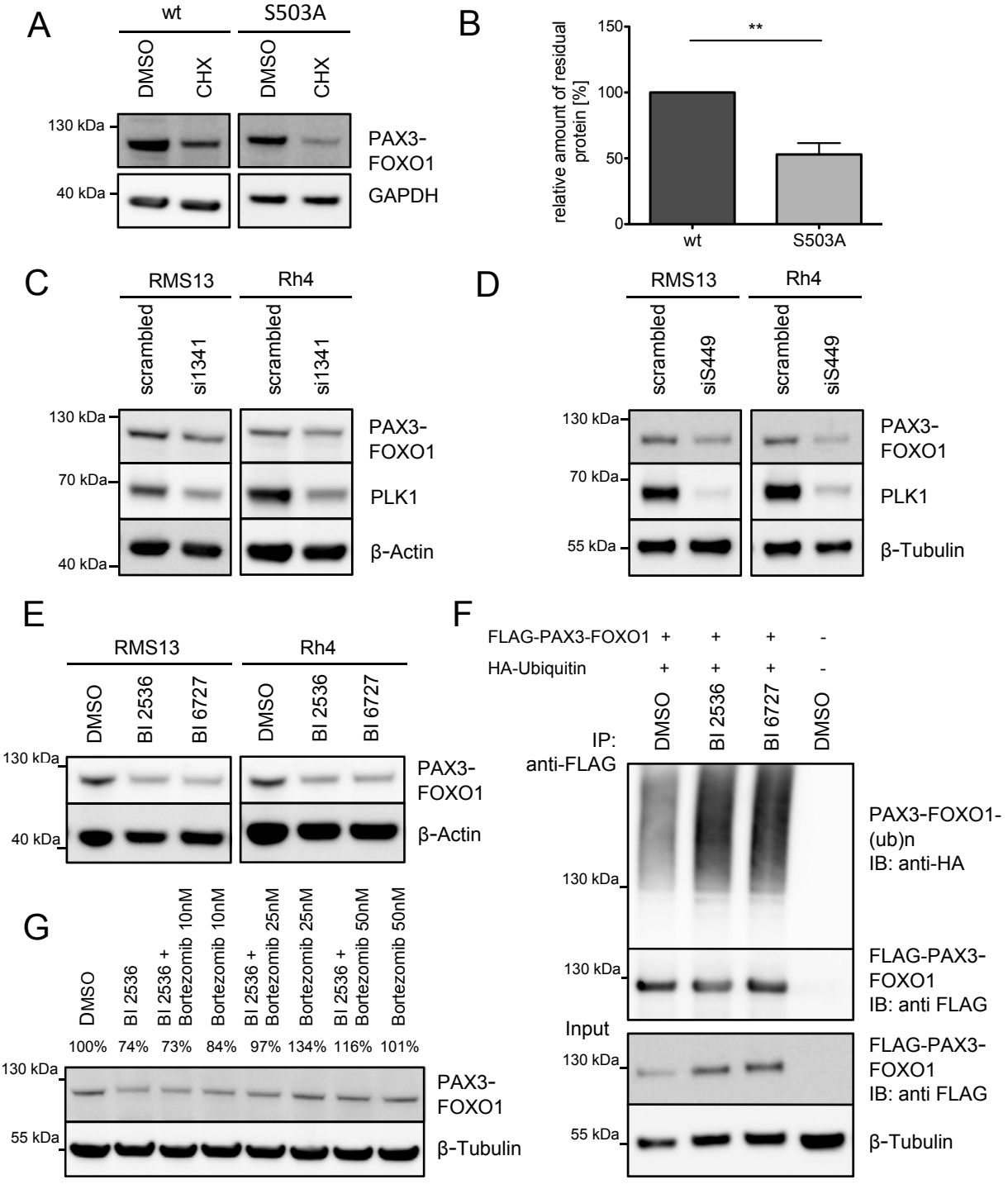
A
wt
S503A
DMSO
CHX
DMSO
CHX
130 kDa
40 kDa
PAX3-FOXO1
GAPDH
B
relative amount of residual protein [%]
150
100
50
0
**
wt
S503A
C
RMS13
Rh4
scrambled
si1341
scrambled
si1341
130 kDa
70 kDa
40 kDa
PAX3-FOXO1
PLK1
β-Actin
D
RMS13
Rh4
scrambled
siS449
scrambled
siS449
130 kDa
70 kDa
55 kDa
PAX3-FOXO1
PLK1
β-Tubulin
E
RMS13
Rh4
DMSO
BI 2536
BI 6727
DMSO
BI 2536
BI 6727
130 kDa
40 kDa
PAX3-FOXO1
β-Actin
F
FLAG-PAX3-FOXO1 + + + -
HA-Ubiquitin + + + -
DMSO
BI 2536
BI 6727
DMSO
IP: anti-FLAG
130 kDa
PAX3-FOXO1-(ub)n
IB: anti-HA
130 kDa
FLAG-PAX3-FOXO1
IB: anti FLAG
Input
130 kDa
FLAG-PAX3-FOXO1
IB: anti FLAG
55 kDa
β-Tubulin
G
DMSO
BI 2536
BI 2536 + Bortezomib 10nM
Bortezomib 10nM
BI 2536 + Bortezomib 25nM
Bortezomib 25nM
BI 2536 + Bortezomib 50nM
Bortezomib 50nM
100% 74% 73% 84% 97% 134% 116% 101%
130 kDa
55 kDa
PAX3-FOXO1
β-Tubulin

Figure 5

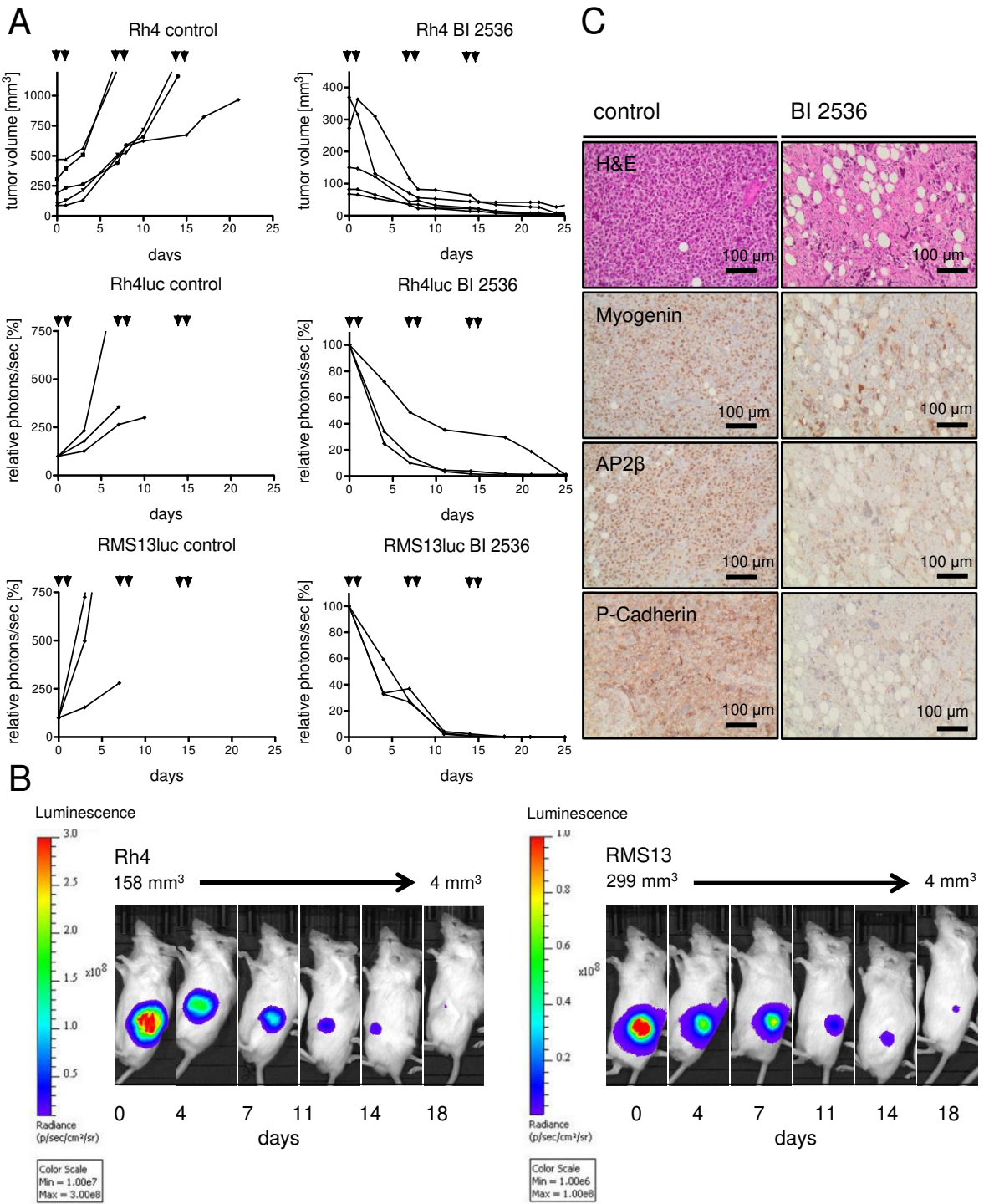
A
Rh4 control
Rh4 BI 2536
tumor volume [mm3]
days
Rh4luc control
Rh4luc BI 2536
relative photons/sec [%]
RMS13luc control
RMS13luc BI 2536
C
control
BI 2536
H&E
Myogenin
AP2β
P-Cadherin
100 µm
B
Luminescence
Rh4
158 mm3
4 mm3
RMS13
299 mm3
x10^8
Radiance (p/sec/cm²/sr)
0 4 7 11 14 18
days
Color Scale
Min = 1.00e7
Max = 3.00e8
Min = 1.00e6
Max = 1.00e8

Figure 6

A

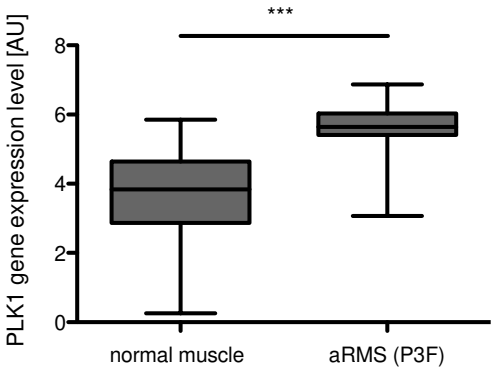

B

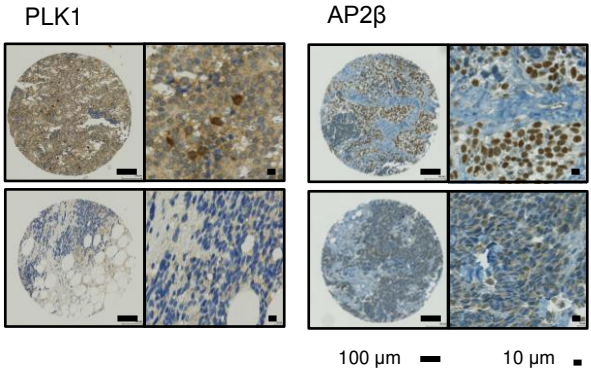

C

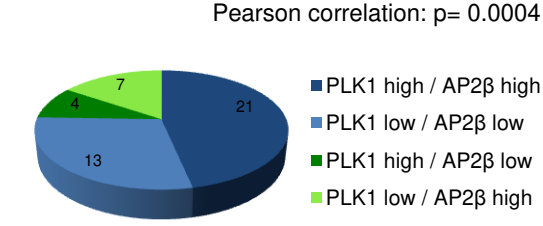

D

PLK1	5yr EFS	95% CI	5yr OS	95% CI
low n=23	42.4%	26.1-68.8%	59.7%	42.4-84.0%
high n=26	15.4%	6.2-37.9 %	20.2%	8.6-47.2%

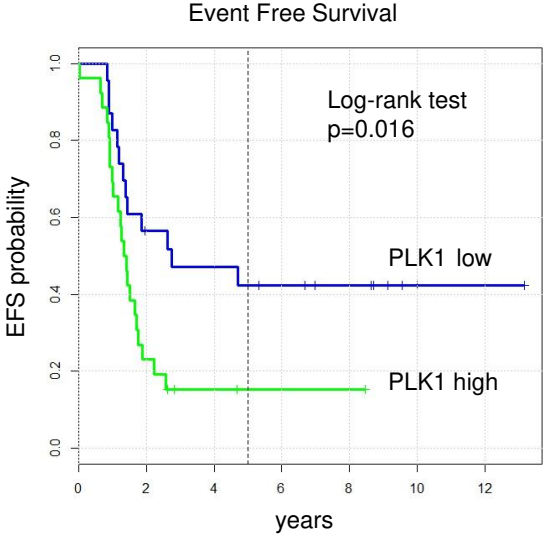

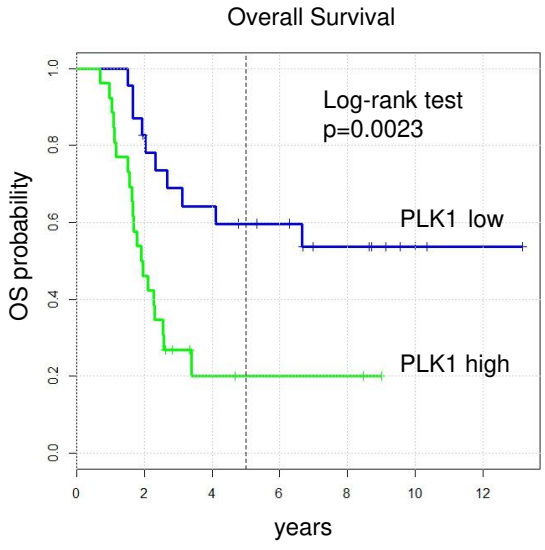

Table 1. Multivariate Analysis

	relative risk	p-value
Event Free Survival		
Age	0.996	0.892
Sex (male vs. female)	0.709	0.367
Localization (unfavorable vs. favorable)	0.704	0.577
PLK1 (high vs. low)	2.340	0.028
Overall Survival		
Age	1.016	0.571
Sex (male vs. female)	0.701	0.392
Localization (unfavorable vs. favorable)	1.230	0.797
PLK1 (high vs. low)	2.560	0.020